Mol Neurobiol
DOI 10.1007/s12035-016-9777-6

Transduction Profile of the Marmoset Central Nervous System Using Adeno-Associated Virus Serotype 9 Vectors

Yasunori Matsuzaki[1] · Ayumu Konno[1] · Ryo Mukai[2] · Fumiaki Honda[3] · Masafumi Hirato[3] · Yuhei Yoshimoto[3] · Hirokazu Hirai[1]

Received: 2 July 2015 / Accepted: 3 February 2016

Abstract The common marmoset is a small New World primate that has attracted remarkable attention as a potential experimental animal link between rodents and humans. Adeno-associated virus (AAV) vector-mediated expression of a disease-causing gene or a potential therapeutic gene in the brain may allow the construction of a marmoset model of a brain disorder or an exploration of the possibility of gene therapy. To gain more insights into AAV vector-mediated transduction profiles in the marmoset central nervous system (CNS), we delivered AAV serotype 9 (AAV9) vectors expressing GFP to the cisterna magna or the cerebellar cortex. Intracisternally injected AAV9 vectors expanded in the CNS according to the cerebrospinal fluid (CSF) flow, by retrograde transport through neuronal axons or via intermediary transcytosis, resulting in diffuse and global transduction within the CNS. In contrast, cerebellar parenchymal injection intensely transduced a more limited area, including the cerebellar cortex and cerebellar afferents, such as neurons of the pontine nuclei, vestibular nucleus and inferior olivary nucleus. In the spinal cord, both administration routes resulted in labeling of the dorsal column and spinocerebellar tracts, presumably by retrograde transport from the medulla oblongata and cerebellum, respectively. Motor neurons and dorsal root ganglia were also transduced, possibly by diffusion of the vector down the subarachnoid space along the cord. Thus, these two administration routes led to distinct transduction patterns in the marmoset CNS, which could be utilized to generate different disease animal models and to deliver therapeutic genes for the treatment of diseases affecting distinct brain areas.

Keywords Common marmoset · Adeno-associated virus serotype 9 vector · Stereology · Cerebellum · Spinal cord · Gene transfer

Introduction

The use of common marmosets (*Callithrix jacchus*) for neuroscience, including both basic and translational research, has been expanding because marmosets have many advantages over macaques, including (1) small size and easy handling, (2) high productive efficiency, and (3) a lack of fatal zoonotic diseases such as herpes B virus [1]. Moreover, marmosets are promising experimental animals that link mice to humans. However, basic neuroanatomical and neurophysiological data are still largely insufficient in marmosets relative to those in macaques.

The abnormal accumulation of neurotoxic proteins in the central nervous system (CNS) causes a variety of disorders, including lysosomal storage diseases [2, 3] and neurodegenerative diseases [4–6]. The efficient transfer of therapeutic genes that ultimately reduce the level of accumulated proteins in neurons of the CNS represents a promising approach for the treatment of these diseases [3, 7–9]. Recent progress in the development of viral vectors has allowed the delivery of transgenes into CNS cells with great efficiency. In particular, adeno-associated virus (AAV) vectors, which are only 20 nm

✉ Hirokazu Hirai
hirai@gunma-u.ac.jp

[1] Department of Neurophysiology and Neural Repair, Gunma University Graduate School of Medicine, Maebashi, Gunma 371-8511, Japan

[2] Department of Ophthalmology, Gunma University Graduate School of Medicine, Maebashi, Gunma 371-8511, Japan

[3] Department of Neurosurgery, Gunma University Graduate School of Medicine, Maebashi, Gunma 371-8511, Japan

Published online: 16 February 2016

in diameter [10], have the potential to transduce broad regions in the CNS [11]. Previous studies used AAV serotype 9 (AAV9) vectors to examine different administration routes in non-human primates (NHPs) such as macaques and marmosets and showed local and retrograde gene transfer in the striatum and visual cortex (marmosets and macaques) [12] and widespread transduction after intravascular and intracisternal administration (macaques) [13–20]. Here, we used marmosets to clarify the transduction profiles and pathways in the CNS after intracisternal or cerebellar parenchymal injection of AAV9 vectors. Our results will be useful for future application of AAV9 vector expression systems to the construction of a marmoset model of a brain disorder as well as neuroanatomical and neurophysiological experiments of marmosets.

Results

Global Transduction of the CNS by Intracisternal Injection of AAV9 Vectors

A previous study showed greater astrocytic tropism of intracisternally administered AAV9 vectors [19]. Because the application of AAV9 vectors for the production of neurodegenerative models and therapeutic gene delivery into neurons are future goals, we used a neuron-specific synapsin I (SynI) promoter. The sequence of the synapsin I promoter is highly conserved among rodents and primates. Therefore, we used 1.0 kb of the rat SynI promoter augmented by the addition of the minimal cytomegalovirus (CMV) promoter (minCMV) sequence (rSynI-minCMV) [21]. The woodchuck hepatitis virus posttranscriptional regulatory element (WPRE) was placed in the main AAV plasmid downstream of the green fluorescent protein (GFP) gene to stabilize the GFP mRNA and increase the expression level of the transgene [22]. An AAV9 vector expressing GFP under the control of the rSynI-minCMV promoter was injected into the cisterna magna of two young adult marmosets approximately 1 year of age (H014 and H017) (Table 1). One marmoset (H014) weighed 250 g and received 150 μl of an AAV9 vector suspension with a titer of 1.5×10^{13} virus genomes (vg)/ml (9.2×10^{12} vg/kg body weight). The second marmoset (H017) weighed 320 g and received 200 μl of an AAV9 vector suspension with a titer of 6.9×10^{13} vg/ml (4.3×10^{13} vg/kg body weight). The behavior of the marmosets after the operation was almost indistinguishable from that of the naïve marmosets. The treated marmosets were euthanized 31 days after viral injection. Observation of whole brains and spinal cords under a fluorescent stereoscopic microscope revealed remarkably diffused GFP expression throughout the CNS (Fig. 1). Then, sagittal (H014) and coronal (H017) sections of the whole brains were produced and double-immunostained for GFP and the Nissl bodies.

Both the sagittal and coronal sections showed strong GFP expression in the medulla oblongata that extended to the cerebellum through the cerebellar peduncle and moderate (or weak) disseminated GFP expression in various brain regions (Fig. 2a–d), such as the cerebral cortex (Fig. 2e), caudate nucleus, hippocampus, the ventral posteromedial nucleus of the thalamus, the gigantocellular reticular nucleus of the medulla oblongata (Fig. 2f), and the cerebellar cortex (Fig. 2g). Interestingly, GFP expression in the cerebral cortex was characterized by a striped pattern that extended from the surface of the cerebral cortex vertically into the cerebral parenchyma. Immunolabeling of blood vessels with an antibody against factor VIII-related antigen showed that the GFP-expressing cells surrounded penetrating arteries (Fig. 2h), suggesting that the AAV9 vectors reached the cerebral parenchyma through the paravascular space (PVS) along the penetrating arteries as previously reported in cynomolgus macaques after AAV9 vector injection into the cisterna magna [19].

Using stereology, we assessed the transduction efficiency in various brain regions by determining the ratio of GFP-expressing neurons to total neurons present in the region of interest (Fig. 2i and Table 2). Consistent with the strong GFP expression observed in the medulla oblongata (low magnification photos; Fig. 2a–d), approximately half of the neurons in the medulla oblongata were transduced by intracisternal injection of the AAV9 vector. Approximately 10–20 % of the neurons in the frontal, parietal, occipital, and temporal lobes of the cerebral cortex, basal ganglia, and cerebellar cortex were transduced, whereas only a small percentage of neurons in the insular lobe, limbic lobe, thalamus, and hypothalamus were transduced (Fig. 2i and Table 2). In the cerebellum, the large projection neurons in the deep cerebellar nuclei (DCN) were efficiently transduced (approximately 50 %), followed by Purkinje cells (approximately 20 %). In contrast, the interneurons with small cell bodies in the DCN and the granule cells in the cerebellar cortex were rarely transduced.

Absence of Purkinje Cell Transduction by Intraparenchymal Injection of an AAV9 Vector With an rSynI-minCMV Promoter

To examine the transduction area and efficiency of the administration of the AAV9 vector directly into the interstitial space of the cerebellum, an AAV9 vector expressing GFP under the control of the rSynI-minCMV promoter was injected into the bilateral cerebellar hemispheres of an adult marmoset (I4222; Table 1). The marmoset received 100 μl (50 μl/hemisphere) of an AAV9 vector suspension with a titer of 3.0×10^{13} (vg)/ml (8.8×10^{12} vg/kg body weight). The treated marmoset was euthanized 555 days after the viral injection. Observation of the whole brain and spinal cord with a fluorescent stereoscopic microscope showed remarkably strong GFP expression in the cerebellum (Fig. 3a, b) and relatively strong GFP

Table 1 Summary of marmosets that received intracisternal and cerebellar parenchymal injections of AAV9 vectors

ID	Route	Gender	Age (year)	Weight (g)	Viral titer (vg/ml)	Volume (μl)	Dose (vg/kg BW)	Sacrifice (days after IJ)	Promoter
H014	IC	M	0.8	250	1.5×10^{13}	150	9.0×10^{13}	31	rSynI-minCMV
H071	IC	F	1.5	320	6.9×10^{13}	200	4.3×10^{13}	31	rSynI-minCMV
I4222	CP	F	5.0	341	3.0×10^{13}	100	8.8×10^{12}	555	rSynI-minCMV
H016	CP	M	1.2	324	1.2×10^{14}	100	3.7×10^{13}	32	MSCV
H018	CP	M	0.9	314	1.2×10^{14}	100	3.8×10^{13}	28	MSCV
H038	CP	F	2.2	341	4.5×10^{13}	100	1.3×10^{13}	30	MSCV

IC intracisternal, *CP* cerebellar parenchymal, *M* male, *F* female, *vg* virus genomes, *BW* body weight, *IJ* injection.

expression along the spinal cord (Fig. 3c, d). Then, coronal sections of the whole brain were produced and double-immunostained for GFP and the Nissl bodies (Fig. 4c–k). These serial coronal sections showed highly efficient GFP expression that occurred bilaterally in the hemispheres and the vermal region of the cerebellum (Fig. 4a). Notably, high magnification images showed an almost complete absence of Purkinje cell transduction throughout the whole cerebellum (Fig. 4c–e, arrowhead), which was in sharp contrast to the strong GFP expression in the granule cells beneath the Purkinje cell layer. Additionally, we observed almost no transduced Purkinje cells in a marmoset treated with an AAV9 vector expressing a different transgene under the control of the rSynI-minCMV promoter (data not shown). These results suggest that little or weak rSynI-minCMV promoter activity occurred in marmoset Purkinje cells.

In addition to the cerebellum, strong GFP expression was observed in several regions of the brainstem and midbrain that were closely associated with the cerebellar cortex, including the red nucleus (Fig. 4b), inferior olivary nuclei (Fig. 4f–h), and pontine nuclei (Fig. 4b, i–k).

Efficient Transduction of Purkinje Cells and Neurons of the Brainstem Nuclei by Intraparenchymal Injection of an AAV9 Vector With the Murine Stem Cell Virus Promoter

Many types of spinocerebellar ataxia (SCA) primarily affect Purkinje cells in the cerebellum [23–25]. Therefore, we were interested in expressing disease-causing and therapeutic genes in Purkinje cells. Because rSynI-minCMV

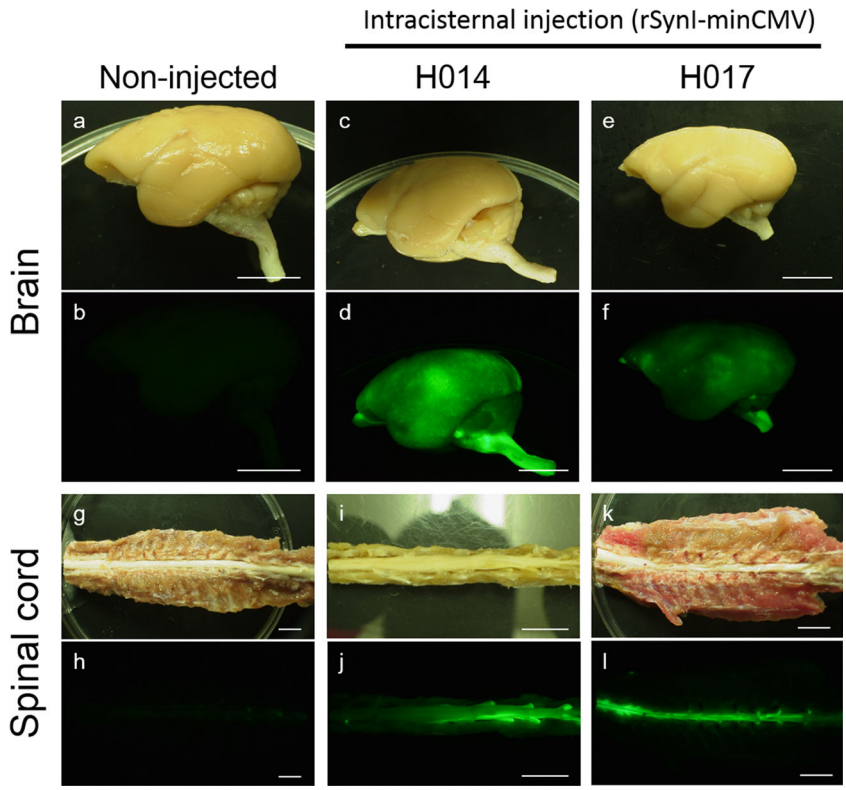

Fig. 1 Global transduction in the marmoset CNS driven by intracisternal injection of an AAV9 vector expressing GFP under the control of the neuron-specific rSynI-minCMV promoter. Whole brains and spinal cords from one non-injected control (Non-injected) and two marmosets (H014 and H017) 1 month after the injection of AAV9 vectors are presented. **a**–**f** Bright field (**a**, **c**, **e**) and GFP fluorescence (**b**, **d**, **f**) images of whole brains from non-injected (**a**, **b**) and AAV9 vector-treated (**c**–**f**) marmosets. **g**–**l** Bright field (**g**, **i**, **k**) and GFP fluorescence (**h**, **j**, **l**) images of spinal cords from non-injected (**g**, **h**) and AAV9 vector-treated (**i**, **k**, **j**, **l**) marmosets (scale bar, 1 cm)

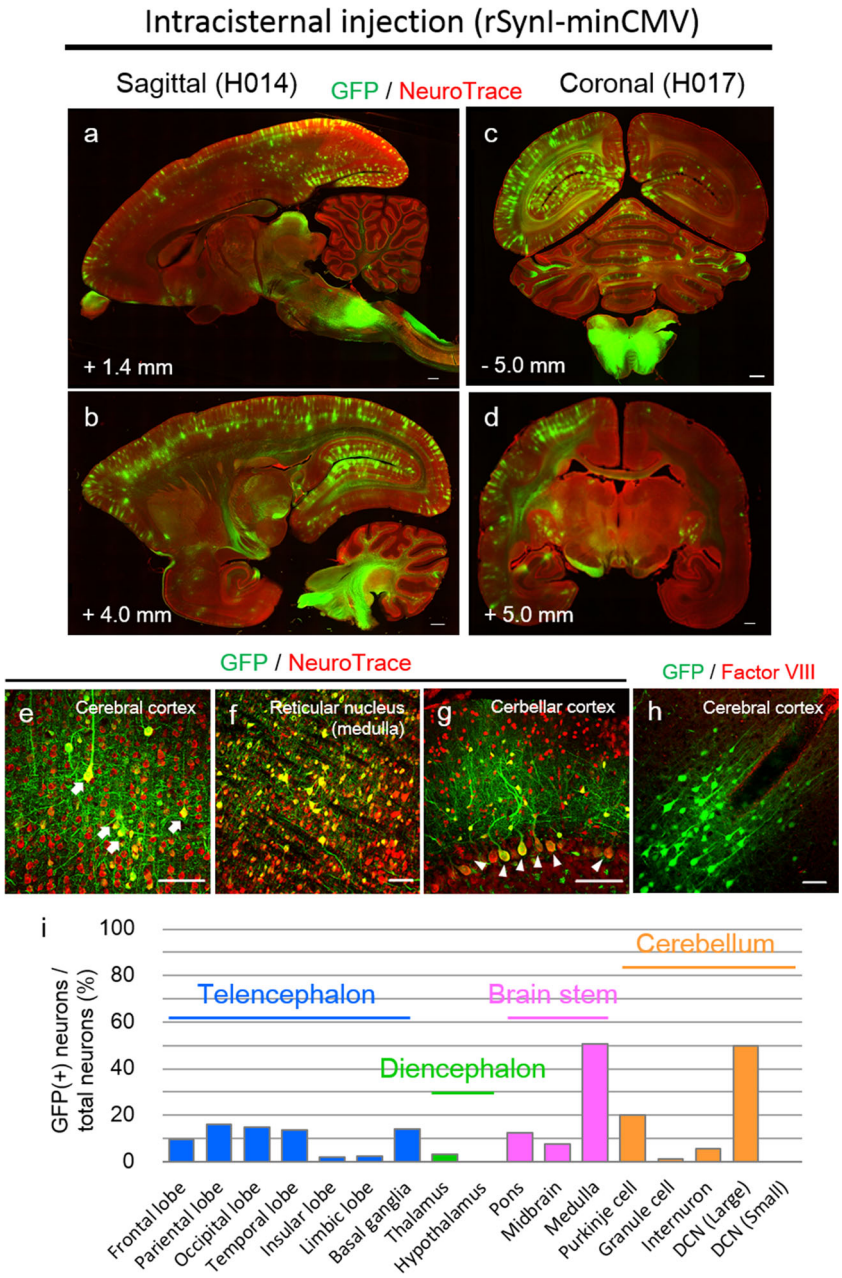

Fig. 2 Whole brain sections from marmosets that received intracisternal injections of an AAV9 vector expressing GFP under the control of the neuron-specific rSynI-minCMV promoter and the transduction efficiency in various brain regions. Sections were immunolabeled for GFP and Nissl bodies (**a**–**g**) or factor VIII-related antigen (**h**). **a**, **b** Sagittal sections +1.4 (**a**) and +4.0 mm (**b**) from the midline. **c**, **d** Coronal sections −5.0 (**c**) and +5.0 mm (**d**) from the bregma. Note the striped GFP expression pattern in the cerebral cortex. **e**–**h** Enlarged images of the cerebral cortex (**e**), reticular nucleus of the medulla oblongata (**f**), and cerebellar cortex (**g**). *Arrows* and *arrowheads* indicate pyramidal neurons and Purkinje cells, respectively. **h** An enlarged image of a GFP stripe in the cerebral cortex, showing many GFP-expressing cells around a blood vessel immunolabeled for factor VIII-related antigen. Scale bars, 1 mm (**a**–**d**) and 100 μm (**e**–**h**). **i** Percent ratios of GFP (+) neurons to total neurons in various brain areas. The number of neurons in each area was determined by stereology. DCN (*large*) and DCN (*small*); large projection neurons and small interneurons, respectively, in the deep cerebellar nuclei

exhibited markedly low promoter activity in the Purkinje cells (Fig. 4c–e), we tested the constitutive murine stem cell virus (MSCV) promoter, which had a preference for Purkinje cells in the mouse cerebellum [26]. AAV9 vectors expressing GFP under the control of the MSCV promoter were injected into the bilateral cerebellar hemispheres of three young adult marmosets (H016, H018, and H038; Table 1). These marmosets received 100 μl (50 μl/hemisphere) of an AAV9 vector suspension with a titer of 1.2×10^{14} vg/ml. The injected marmosets appeared to be slightly ataxic on the day of operation but recovered and were almost indistinguishable from the naïve marmosets by the next day.

The treated marmosets were euthanized approximately 1 month after the viral injection. Observation of the whole brain and spinal cord with a fluorescent stereoscopic microscope showed remarkably strong GFP expression in the cerebellum (Fig. 3e, f, i, j) and relatively strong GFP expression along the spinal cord (Fig. 3g, h, k, i). Sagittal (H018) and coronal (H016) sections of the whole brains were produced and double-immunostained for GFP and the Nissl bodies (Fig. 5a–h). These serial sagittal sections showed that the wide-ranging transduction of the cerebellar cortex and white matter occurred primarily from the anterior to the central lobules (Fig. 5a, b), whereas the serial coronal sections showed efficient GFP expression in the whole cerebellum (Fig. 5c).

Table 2 Number of GFP-positive and total neurons in various regions of the marmoset brain

Intracisternal injection (rSynl-minCMV promoter)[a]

	Telencephalon							Diencephalon		
	Frontal lobe	Pariental lobe	Occipital lobe	Temporal lobe	Insular lobe	Limbic lobe	Basal ganglia	Thlaramus	Hypothalamus	
GFP(+)	7,346	9,081	20,204	9,081	102	1,836	9,081	510	0	
GFP(−)	70,408	47,755	116,938	58,163	5,510	78,163	55,408	16,122	13,061	
Total	77,754	56,836	137,142	67,244	5,612	79,999	64,489	16,632	13,061	
	Brainstem			Cerebellum					White matter	Total
	Pons	Midbrain	Medulla	Purkinje cell	Granule cell	Interneurons	DCN (Large)	DCN (Small)		
GFP(+)	408	306	2,959	306	4,693	816	102	0	510	67,341
GFP(−)	2857	3673	2,875	1,224	390,612	13,775	102	1,734	57,653	936,015
Total	3206	3979	5,816	1,530	395,305	14,591	204	1,734	58,163	1,003,358

Cerebellar parenchymal injection (MCSV promoter)[b]

	Cerebellum						
	Purkenji cell	Granule cell	Interneurons in GCL	Interneurons in ML	Neurons in WM	Large neurons in DCN	Small neurons in DCN
GFP(+)	962	5,722	542	9,502	892	17	612
GFP(−)	210	190,644	4,025	17,062	7,175	105	5,687
Total	1172	196,366	4,567	26,564	8,067	122	6,299
	Vestibular nucleus		Inferior olivary nucleus		Pontine nuclei		
	Large neurons	Other neurons	Large neurons	Other neurons	Large neurons	Other neurons	
GFP(+)	159	121	218	29	167	29	
GFP(−)	156	1,473	91	702	64	330	
Total	315	1,594	309	731	231	359	

Neurons were identified by NeuroTrace labeling, and the number ($\times 10^3$) was determined by stereology. Each value is the average of two AAV9 vector-injected marmosets

DCN deep cerebellar nuclei, *GCL* granule cell layer, *ML* molecular layer, *WM* white matter

[a] Results obtained from two marmosets following the intracisternal injection of an AAV9 vector expressing GFP under the control of the neuron-specific rSynI-minCMV promoter

[b] Results obtained from two marmosets following cerebellar parenchymal injection of an AAV9 vector expressing GFP under the control of the MSCV promoter

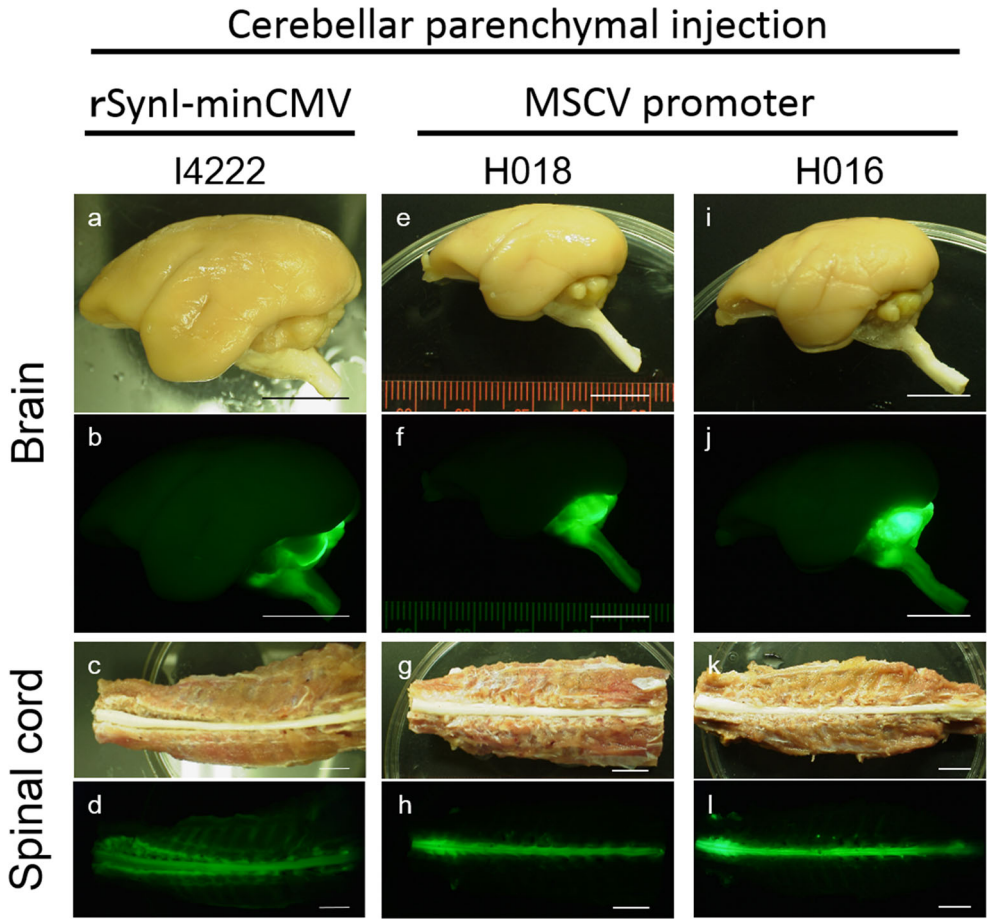

Fig. 3 Robust transduction of the cerebellum, brainstem, and spinal cord by cerebellar parenchymal injection of an AAV9 vector. AAV9 vectors expressing GFP under the control of the rSynI-minCMV or MSCV promoter were injected bilaterally into the cerebellar hemispheres of adult marmosets (I4222, H018, and H016). The GFP expression profiles in the brain and spinal cord were examined 1.5 years (rSynI-minCMV) or 1 month (MSCV promoter) after viral injection. The bright field and GFP fluorescent images from I4222 (**a**–**d**), H018 (**e**–**h**), and H016 (**i**–**l**) are presented (scale bar, 1 cm)

We produced coronal sections of the brain from another marmoset (H038) that showed a transduction pattern similar to H016 (data not shown). A major difference in the transduction patterns between the rSynI-minCMV and MSCV promoters is the robust and efficient transduction of Purkinje cells by the MSCV promoter (Fig. 5e), which is in contrast to the almost complete lack of Purkinje cell transduction by the rSynI-minCMV promoter (Fig. 4c–e). However, the brainstem and midbrain, which are closely associated with the cerebellar cortex, expressed GFP at levels similar to the rSynI-minCMV promoter in regions including the vestibular nuclei, inferior olivary nuclei, pontine nuclei, and red nucleus (Fig. 5a, f–h). Moreover, GFP expression was lower but clearly present in regions that received cerebellar efferents, such as the thalamic nuclei (LP, VPL, VPPC, and VPM) [27] and dorsal lateral geniculate nucleus (DLG) [28] (Fig. 5b, d). Interestingly, the visual cortex (V1–V3) expressed GFP (especially V2 and V3) (Fig. 5b); these regions are also connected to the cerebellum by a pontine nuclear relay [29].

Using stereology, we assessed the transduction efficiency of neurons in various cerebellar regions by determining the ratio of GFP-expressing neurons to total neurons present in the region of interest (Fig. 5m and Table 2). Notably, more than 80 % of the Purkinje cells (Fig. 5e, m) and 50–70 % of the large projection neurons in the vestibular nucleus (Ve) (Fig. 5f, m), inferior olivary nucleus (Fig. 5g, m), and pontine nuclei (Fig. 5h, m) expressed GFP, whereas only limited percentages of granule cells (Fig. 5m) and neurons in the DCN expressed GFP, including large projection neurons and small interneurons (Fig. 5m).

Efficient Transduction of Motor Neurons and Sensory Afferents in the Spinal Cord by Intracisternal and Cerebellar Parenchymal Injection of the AAV9 Vector

The transduction profiles of the spinal cord were examined at different spinal levels by double-immunolabeling of transverse sections for GFP and choline acetyltransferase. The fluorescent microscopic images revealed that similar components were labeled by GFP following both intracisternal injection and cerebellar parenchymal injection. The AAV9 vector transduced motor neurons in the anterior horns, dorsal root ganglia cell bodies, and sensory projections, such as the dorsal column medial lemniscus, spinocerebellar tracts, and spino-olivary fibers (Fig. 6). These GFP-expressing sensory afferents projected into the brainstem and cerebellum, both of which were close to the viral injection sites. These results suggested the

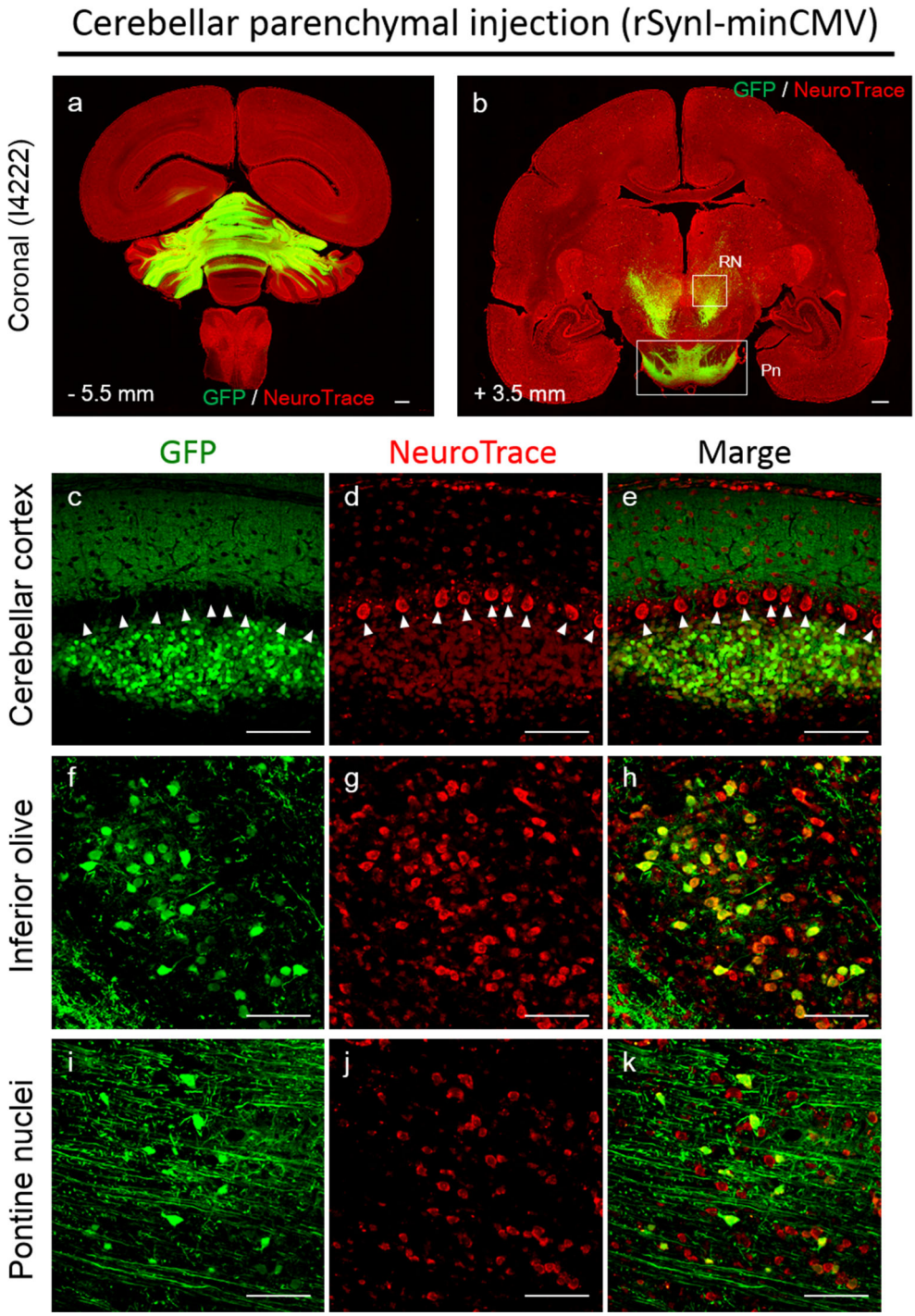

Fig. 4 Coronal sections of the whole brain and the magnified images following cerebellar parenchymal injection of an AAV9 vector expressing GFP under the control of the neuron-specific rSynI-minCMV promoter. Sections were immunostained for GFP and Nissl bodies. **a**, **b** Coronal sections −5.5 (**a**) and +3.5 mm (**b**) from the bregma. *Pn*, pontine nuclei; *RN*, red nucleus. Note the high levels of GFP expression in the cerebellum and areas relevant to the cerebellar cortex. **c**–**k** Enlarged images of the cerebellar cortex (**c**–**e**), inferior olivary nucleus (**f**–**h**) and pontine nuclei (**i**–**k**). GFP, NeuroTrace, and the merged images were presented as depicted. Note the complete absence of GFP expression in the Purkinje cells (*arrowheads*). Scale bars, 1 mm (**a**, **b**) and 100 μm (**c**–**k**)

occurrence of retrograde transport and the consequent transduction of neurons whose axons constituted the dorsal column medial lemniscus, spinocerebellar tracts, and spino-olivary fibers (Fig. 6). In addition to the lower motor neurons and dorsal root ganglia, we examined the retinas of marmosets as an example of peripheral neuronal structures after intracisternal or cerebellar parenchymal injection but found no GFP-positive cells (data not shown).

Discussion

AAV is non-pathogenic for humans and measures only 20–25 nm in diameter [10]. Thus, AAV9 vectors are diffusible in the brain and allow the efficient delivery of transgenes to broad regions of the CNS. These advantages allow the use of AAV9 vectors for the generation of disease model animals for the study of neurodegenerative diseases [30, 31] and gene therapy vectors that may target brain disorders [8, 32, 33]. For these

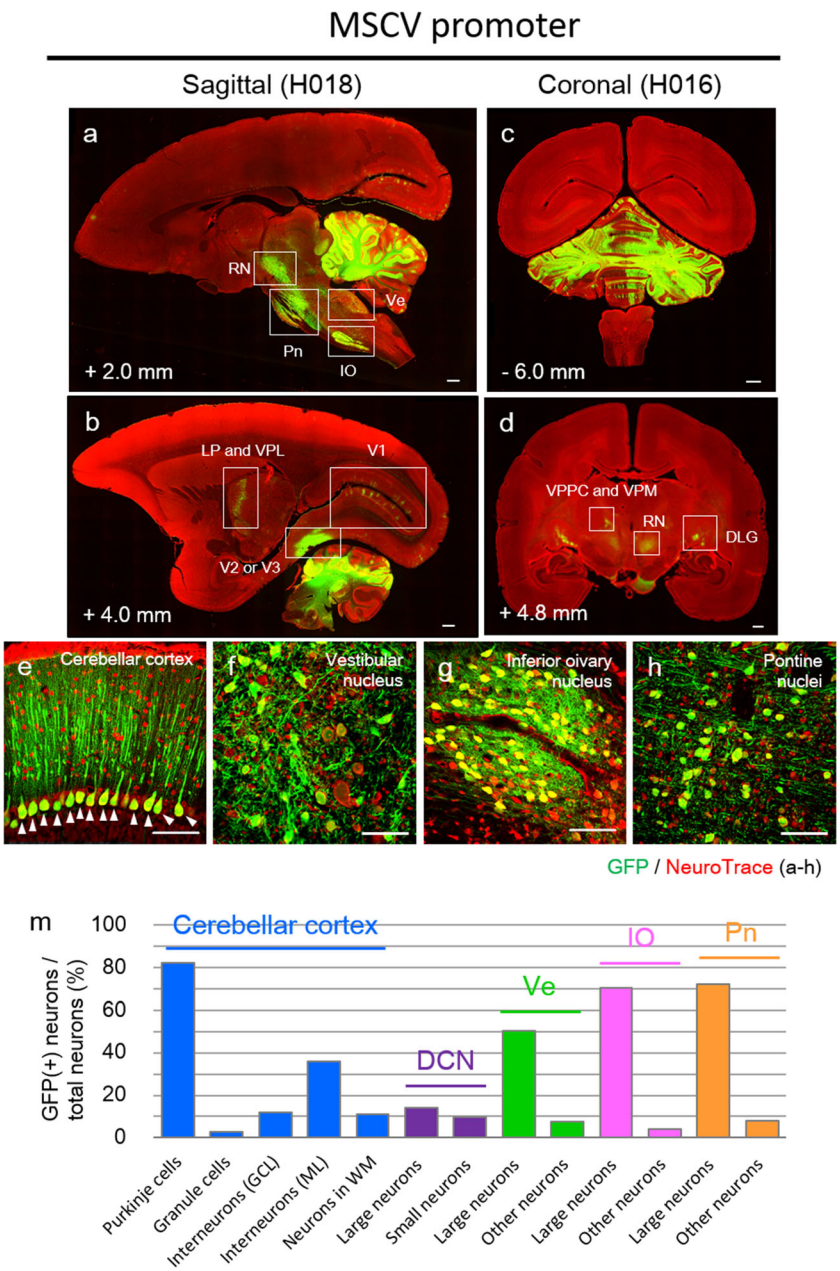

Fig. 5 Whole brain sections following cerebellar parenchymal injection of an AAV9 vector expressing GFP under the control of the MSCV promoter and the transduction efficiency in the cerebellum and the areas associated with the cerebellum. Sections were immunostained for GFP and Nissl bodies. **a** Sagittal sections +2.0 mm from the midline. *IO*, inferior olive; *Pn*, pontine nuclei; *RN*, red nucleus; *Ve*, vestibular nucleus. **b** Sagittal sections +4.0 mm from the midline. *V1–V3*, visual area (1–3); *LP*, lateral posterior thalamic nucleus; *VPL*, ventral posterolateral thalamic nucleus. **c**, **d** Coronal sections −6.0 mm (**c**) and +4.8 mm (**d**) from the bregma. *DLG*, dorsal lateral geniculate nucleus; *RN*, red nucleus; *VPM*, ventral posteromedial thalamic nucleus; *VPPC*, ventral posterior nucleus of the thalamus, parvicellular. Note the high levels of GFP expression in the cerebellum and areas relevant to the cerebellar cortex. **e**–**h** Enlarged images of the cerebellar cortex (**e**), vestibular nucleus (**f**), inferior olivary nucleus (**g**), and pontine nuclei (h). Scale bars, 1 mm (**a**–**d**) and 100 μm (**e**–**h**). **i** Percent ratios of GFP (+) neurons to total neurons in the cerebellum and brain stem areas associated with the cerebellar cortex. The number of neurons was determined by stereology. *DCN*, deep cerebellar nuclei; *GCL*, granule cell layer; *IO*, inferior olive; *ML*, molecular layer; *Pn*, pontine nuclei; *Ve*, vestibular nucleus; *WM*, white matter

applications, it is important to clarify the relationship between the administration route of the AAV9 vector and the consequent transduction profiles in the CNS. Although such experiments have been primarily conducted in rodents [30, 34–36], there are significant merits to using NHP to replicate human disease pathology and to assess the benefits and adverse reactions that accompany therapeutic gene delivery.

Cerebrospinal fluid (CSF) is produced at the choroid plexus and flows through the cerebral ventricles and subarachnoid space [37–39]. A recent study demonstrated that CSF flowed

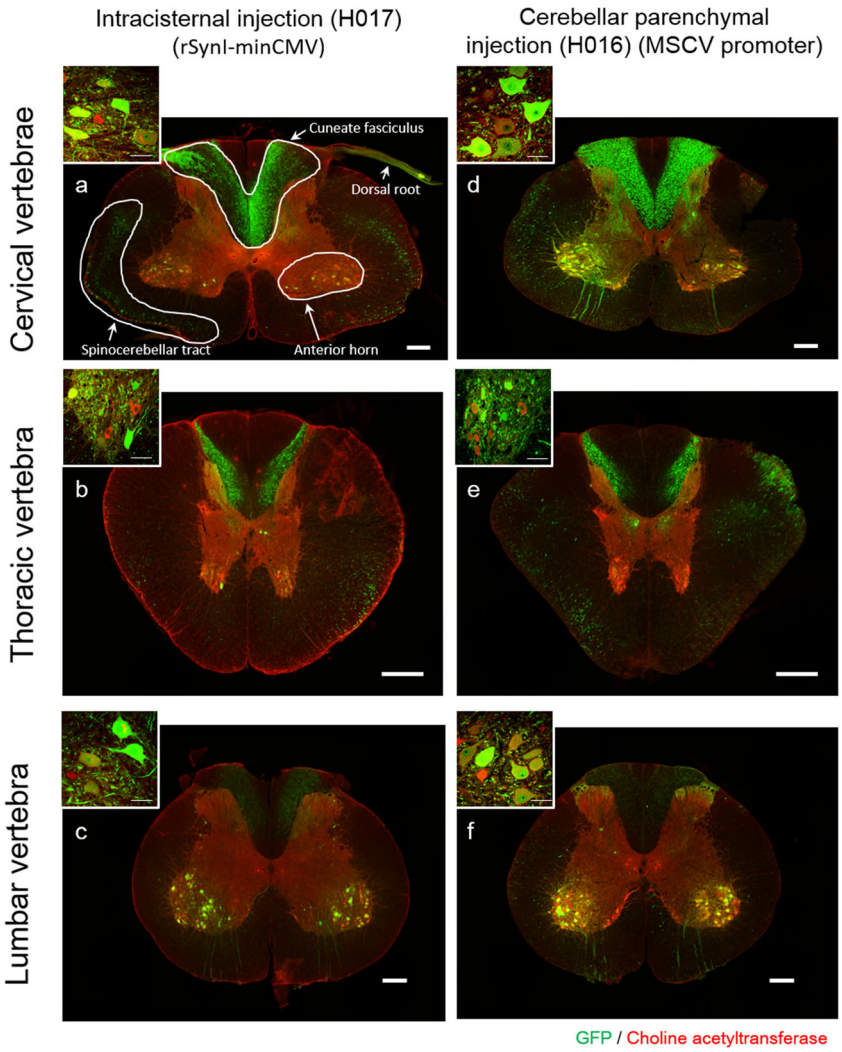

Fig. 6 Immunohistochemistry of the spinal cord at different levels. Transverse sections of the cervical (**a**, **d**), thoracic (**b**, **e**), and lumbar (**c**, **f**) cords from marmosets following intracisternal (H017), and cerebellar parenchymal (H016) injection were double-immunolabeled for GFP (*green*) and choline acetyltransferase (*red*). The inset in each panel is an enlarged view of the ventral horn showing efficient GFP expression in motor neurons immunolabeled for choline acetyltransferase (scale bars, 300 and 50 μm (*insets*))

into the PVS surrounding the arteries that penetrate the brain tissue [40]. Intracisternally administered AAV9 vectors diffused via the CSF and flowed in the PVS that surrounded the arteries entering the brain tissue. The inner and outer walls of the PVS consist of vascular smooth muscle and astrocytic endfeet, respectively. CSF is actively transferred from the PVS to the interstitial space by the aquaporin 4 protein present on the endfeet [40], whereas the AAV9 vectors must pass through the cleft between endfeet to reach the brain tissue. Because the astrocytic processes of primates are far more complex than those of rodents [41], the distance between the endfoot gap and the permeability of the AAV9 vectors through it may differ between primates and rodents. To answer these questions, we performed AAV9 experiments in marmosets.

We administered AAV9 vectors to the marmoset CNS via two different injection routes (intracisternal and cerebellar parenchymal). To reach the brain parenchyma, intracisternally injected AAV9 vectors flowing in the CSF have to pass the endfoot gap, which is presumably 20 nm or less in NHPs. This reduced gap suggests that only a portion or none of the AAV9 vector may reach the brain tissue. The limited (striped) transduction along the penetrating arteries in the cerebral cortex (Fig. 2a–d) suggests that the gap between the astrocytic endfeet is permeable for the AAV9 vectors but that the permeability is not very high. In the parenchymal injection, AAV9 vectors are administered directly into the interstitial space, resulting in transduction of almost the entire cerebellar cortex (Fig. 7b, red arrow). Neurons in the inferior olivary nuclei, pontine nuclei, and vestibular nuclei were highly efficiently transduced (50–70 % of the projection neurons, Fig. 5m). This result could be explained by the infection of AAV9 vectors from the axon terminals projecting into the cerebellar cortex and the subsequent retrograde transport (Fig. 7b, blue arrow).

The finding that intracisternal injection and cerebellar parenchymal injection resulted in essentially the same transduction patterns in the spinal cord was unexpected. Because both administration routes robustly transduced the cerebellar cortex and the medulla oblongata, we postulated that the neurons whose axons constituted the dorsal column medial lemniscus and spinocerebellar tracts were retrogradely transduced by

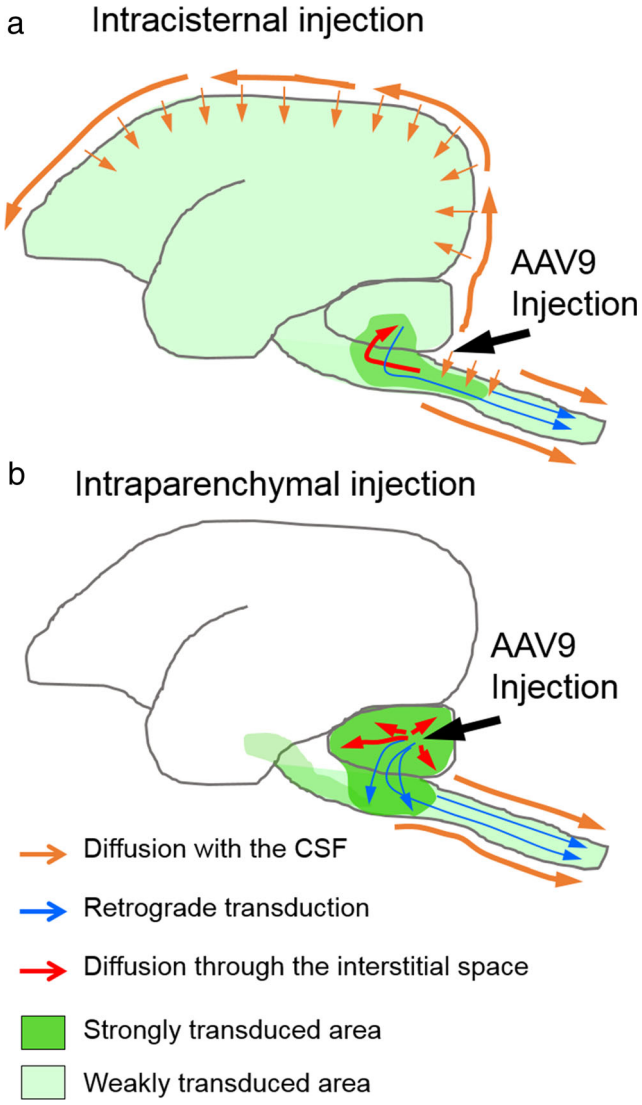

Fig. 7 Schematic depicting a possible diffusion route of AAV9 vectors in the marmoset CNS. **a** Intracisternally injected AAV9 vectors primarily expand with the CSF flow (*thick orange arrow*) and enter into the paravascular space (PVS) along arteries penetrating into the cerebral tissue. A portion of the AAV9 particles pass through the astrocytic endfoot gap to enter the interstitial space and transduce neurons near the penetrating arteries (*thin orange arrow*). Some AAV9 vectors enter the interstitial space of the brainstem close to the injection site, probably due to the high viral density, and diffuse through the interstitial space to reach the cerebellum (*red arrow*). Neurons in the spinal cord are transduced by two different routes: the first is retrograde transport from axon terminals projecting into the cerebellum (spinocerebellar tract) and brainstem (cuneate fasciculus) (*blue arrow*) and the second is infection by AAV9 vectors diffusing into the subarachnoid space along the spinal cord (*thick orange arrow*), leading to the retrograde transport and transduction of motor neurons and neurons of the dorsal root ganglia. **b** Cerebellar parenchymal injection causes diffusion of AAV9 vectors into the interstitial space throughout the cerebellar cortex (*red arrow*). Relevant brainstem nuclei are efficiently transduced in a retrograde fashion (*blue arrow*). Neurons in the spinal cord are transduced similarly to those intracisternally injected with AAV9 vectors (i.e., retrograde transport via axons projecting into the cerebellum (spinocerebellar tract) and brainstem (cuneate fasciculus) (*blue arrow*)). The vectors that diffuse through the subarachnoid space (*orange arrow*) are re-retrogradely transported through the axons of motor neurons and dorsal root ganglia. Color figure online

infection with AAV9 vectors from the axon terminals in the medulla oblongata and cerebellum (Fig. 7a, b, blue arrow). In contrast, motor neurons in the ventral horn and dorsal root ganglia were presumably transduced in a manner that differed from the dorsal column and spinocerebellar tracts; considering the preference of AAV9 vectors for retrograde transport, the vectors descending in the subarachnoid space along the spinal cord most likely infected the axons of motor neurons and dorsal root ganglia and were retrogradely transported to transduce those neurons.

It is likely that the similar administration of AAV9 vectors results in different transgene expression patterns in rodents and other species because the affinity of AAV9 vectors for neurons and glia may differ among species. Moreover, it is highly probable that the activities of the cell type-specific promoters used to drive gene expression in the AAV9 vectors differ between rodents and other species, including primates. Therefore, a number of studies have aimed to clarify the transduction profiles of AAV vectors in different species, such as cynomolgus macaques [13, 16–19], rhesus macaques [14], pigs [13, 42], and cats [20]. Most of these studies employed intracisternal injection [13, 16–20]. The administration of the AAV9 vector into the cisterna magna of marmosets in this study was basically similar to studies that used cynomolgus macaques in terms of global transduction and transduced cell types, such as spinal motor neurons [16–18], dorsal root ganglia [18], and cerebral pyramidal neurons close to the blood vessels [16, 18, 19]. It is difficult to compare retrograde transport between marmosets and other animals because previous studies have not described the transduction pathway in detail. One detectable difference between marmosets and cynomolgus macaques is marked GFP expression in the dorsal column-medial lemniscus pathway (sensory afferents) in marmosets (Fig. 6) but not in cynomolgus macaques. In contrast, high transduction was observed in the descending ventral corticospinal tracts in cynomolgus macaques [18]. Transduction of the sensory afferents in marmosets is thought to occur by the invasion of the medulla oblongata by high density AAV9 vectors, leading to retrograde axonal transport through the dorsal column. Therefore, the absence of spinal cord transduction in cynomolgus macaque may be attributable to the lower density of AAV9 vectors in the medulla oblongata due to rapid viral diffusion in the CSF rather than entry into the medulla.

GFP fluorescence image from the marmoset (H014) treated with lower titer AAV9 vectors (Fig. 1d) was brighter than that from the marmoset (H017) treated with higher titer vectors (Fig. 1f). We postulate that the posture after the viral injection substantially influenced the viral diffusion in the CSF and consequent transduction pattern. Indeed, the Trendelenburg position after viral injection was shown to facilitate spreading of the vector and significantly increase the transduction efficacy in cynomolgus macaques [17].

Many previous studies used constitutive promoters that were active in almost all cell types, such as the CMV promoter and CMV early enhancer/chicken β actin (CAG) promoter. In contrast, we used a neuron-specific rSynI-minCMV promoter and the constitutive MSCV promoter and found that the rSynI-minCMV promoter had no or very weak promoter activity in marmoset Purkinje cell (Fig. 4c–e), although this promoter exhibited robust promoter activity in mouse Purkinje cell [21, 30]. Thus, we have to be cautious in choosing promoters (especially cell type-specific promoters) because they can behave quite differently in monkeys and presumably in humans compared with rodents.

The present results suggest that intracisternal injection is suitable for diffuse and global transduction of the CNS, whereas cerebellar parenchymal injection leads to more limited and robust transduction of the cerebellar cortex and cerebellar efferent neurons. Both administration routes transduced motor neurons, dorsal root ganglia, the dorsal column medial lemniscus and spinocerebellar tracts. The former route could be utilized for gene therapy against diseases affecting broad brain areas, such as Alzheimer's disease and mucopolysaccharidosis, whereas the latter route may be of use for gene therapy against disorders that primarily impair the cerebellum, the associated brainstem nuclei, and the spinal cord, such as spinocerebellar degeneration.

Materials and Methods

Marmosets

We used six common marmosets (*C. jacchus*; three males and three females) in this study. Marmosets were purchased through CLEA Japan (Tokyo, Japan) and were bred at the Gunma University Bioresource Center. The animals were maintained in rooms under controlled temperature (25 to 27 °C), humidity (40 to 50 %), and light cycle (12 h each of light and dark) conditions. Water was provided ad libitum, and 40 to 50 g of soaked monkey chow (CMS-1, CLEA Japan) with vitamin supplementation and fruit, boiled chicken or milk powder was provided daily. All efforts were made to minimize suffering and reduce the number of animals used.

Construction of Plasmids and AAV9 Production

We used two expression plasmids (pAAV-MSCV-GFP and pAAV-rSynI-minCMV-GFP-WPRE) [21] for AAV9 vector production. pAAV-MSCV-GFP was generated by subcloning the MSCV-GFP fragment from pCL20c-MSCV-GFP [43] into pAAV. The following two primer pairs were used to amplify the inserts: XhoI-MSCV (forward) 5′-CGACTCGAG TAACGGGCCCAGCTTCGA-3′/GFP (reverse) 5′-GTTTAAACTCATTACTTGTACAGCTCGTCCATG-3′ and XhoI-rSynI (forward) 5′-ATGCTCTAGACTCG AGGAAGAGGCTGAATACACATCAGAG-3′/KpnI-WPRE (reverse) 5′-CTAGAGGATCCCCGGGTACCA TGCGGGGAGGCGGCCCAAA-3′.

The AAV9 vectors were produced as previously described [44]. Briefly, AAV9 vectors were generated by the cotransfection of HEK293T cells (Thermo Fisher Scientific, Waltham, MA, USA) with three plasmids: pHelper (Stratagene, La Jolla, CA, USA), pAAV2/9 (kindly provided by Dr. J. Wilson), and one of the two expression plasmids. The viral particles were purified using ammonium sulfate precipitation and iodixanol continuous gradient ultracentrifugation as previously described [45]. The genomic titer of the purified AAV9 vectors (Table 1) was determined by quantitative real-time PCR (Dice TP800, Takara Bio, Shiga, Japan) using the THUNDERBIRD SYBR qPCR Mix (Toyobo, Osaka, Japan) with the following primers: 5′-CTGTTGGGCACTGACAATTC-3′ and 5′-GAAGGGACGTAGCAGAAGGA-3′ targeting the WPRE sequence, or 5′-CACTCCCTTAAGTTTGACCTT-3′ and 5′-GCCAAGGCTTCCCAGGTC-3′ targeting MSCV.

Viral Vector Injection

AAV9 vectors were injected into the cisterna magna or cerebellar cortex. Marmosets were anesthetized with ketamine (20–25 mg/kg) and xylazine (1.6–2.0 mg/kg), and anesthesia was maintained by inhalation of 2.0–2.5 % isoflurane (air flow, 0.5 l/min) in 80–100 % O_2. The hair in the occipital region was shaved prior to the skin incision. A 30-gauge needle attached to a 1-mm syringe was inserted into the cisterna magna through the dura mater and arachnoid; the needle tip was monitored by radioscopy. We confirmed the entrance of the needle tip into the subarachnoid space by gentle suction of CSF into the syringe. Then, the syringe was replaced with a syringe containing the AAV9 vector, and 150 μl (H014) or 200 μl (H017) of the viral suspension was injected into the cisterna magna.

For viral injection into the cerebellar parenchyma, the marmosets were fixed with a stereotaxic apparatus (SR-6C-HT; Narishige, Tokyo, Japan). Muscles and ligaments over the occipital bone were carefully pushed aside without cutting to expose the occipital bone. The bone was pierced using a 25-gauge needle (4.0 mm caudal to the torus occipitalis and 3.5–4.0 mm lateral to the midline). The AAV9 vector was injected bilaterally into the cerebellar hemispheres (5.0 mm deep from the occipital bone surface). Fifty microliters of the viral solution was injected unilaterally into the hemisphere at a speed of 5 μl/min for 10 min using a 33-gauge Hamilton syringe and a micropump (UltramicroPump II; World Precision Instrument, Sarasota, FL, USA).

Histological Analysis

The marmosets were deeply anesthetized with a combination of ketamine, xylazine, and isoflurane and transcardially

perfused with 1× phosphate-buffered saline (PBS(−)) and a fixative containing 4 % paraformaldehyde in 0.1 M phosphate buffer. Native GFP fluorescent images of whole brains were obtained with a fluorescence stereoscopic microscope (VB-7010; Keyence, Osaka, Japan). Then, the brains and spinal cords were cut into 100-μm-thick sections using a Vibrating Blade Microtome (VT1000; Leica, Wetzlar, Germany). The eyes were cut into 8-μm-thick sections using the Cryostat (CM3050; Leica).

Immunohistochemistry

Sections were immunostained for GFP and Nissl bodies or choline acetyltransferase. Blood vessels in the cerebral cortex were visualized by immunolabeling for Factor VIII. Floating brain and spinal cord sections were incubated in blocking solution (2 % bovine serum albumin, 2 % normal donkey serum (S30-100 ml; Merck Millipore, Billerica, MA, USA) and 0.4 % Triton X-100 in 0.1 M phosphate buffer) for 1 day at 4 °C with the following primary antibodies: rat monoclonal anti-GFP (1:1000; 04404–84; Nacalai Tesque, Kyoto, Japan), rabbit polyclonal anti-Factor VIII-related antigen (von Willebrand factor) (1:2; 220 M; Biomeda, Foster City, CA, USA), and goat polyclonal anticholine acetyltransferase (1:100; AB144P; Merck Millipore). The bound primary antibodies were visualized after incubation with Alexa Fluor 488-conjugated donkey anti-rat IgG (1:1000; Thermo Fisher Scientific), Alexa Fluor 594-conjugated donkey anti-rabbit IgG (1:1000; Thermo Fisher Scientific), and Alexa Fluor 568-conjugated donkey anti-goat IgG (1:1000; Thermo Fisher Scientific) in blocking solution for 2 h at room temperature. After the secondary antibody reaction, Nissl bodies were stained with NeuroTrace 530/615 (1:200; Thermo Fisher Scientific) or NeuroTrace 640/660 (1:200; Thermo Fisher Scientific) in PBS for 1 h at room temperature. The immunostained sections were mounted in the ProLong Gold or Diamond antifade reagent (Thermo Fisher Scientific). Low magnification images of the whole brain and spinal cord sections were obtained using fluorescence microscopes (BZ-9000 or BZ-X700, Keyence). High-magnification images were obtained using a confocal laser scanning microscope (LSM 5 PASCAL; Carl Zeiss, Oberkochen, Germany).

Stereology

The number and efficiency of GFP-expressing neurons in various brain regions were analyzed statistically by stereology using Stereo Investigator ver. 11 (Micro Bright Field Japan, Chiba, Japan). Following intracisternal injection, a 1-in-20 series (1 section per 2.0 mm) of 17 sections immunostained for GFP and Nissl bodies (NeuroTrace) were analyzed. The counting grid was 2500 × 2500 μm, the counting frame was 35 × 35 μm, and the dissector height was 30 μm.

For the brains that received a cerebellar parenchymal injection, the cerebellum and brainstem were analyzed using different counting frames and grid sizes. For the examination of the cerebellum, the interval was 1.2 mm (1-in-12 series, six sections), the counting grid was 3500 × 2500 μm, the counting frame was 100 × 100 μm, and the dissector height was 30 μm. For the examination of the brainstem, the interval was 0.5 mm (1-in-5 series), the counting grid was 300 × 300 μm, the counting frame was 35 × 35 μm, and the dissector height was 30 μm. The inferior olivary nucleus, pontine nuclei, and vestibular nucleus were examined using five, four, and seven sections, respectively.

To determine the ratio of GFP-expressing neurons to total neurons present in the examined brain regions, neurons double-labeled for GFP and Nissl bodies (NeuroTrace) and neurons labeled only with NeuroTrace were counted independently, and the ratios were calculated. In total, 9788 neurons were counted for the intracisternal injection, and 13,895, 710, 258, and 830 neurons were counted in the cerebellum, inferior olivary nucleus, pontine nuclei, and vestibular nucleus, respectively, for the cerebellar parenchymal injection.

Acknowledgments The authors are very grateful to the technicians Motoko Uchiyama and Minako Noguchi for raising the marmosets. This research is (partially) supported by the program for Brain Mapping by Integrated Neurotechnologies for Disease Studies (Brain/MINDS) from the Ministry of Education, Culture, and Sports Science (MEXT) and the Japan Agency for Medical Research and Development (AMED), MEXT KAKENHI grant number 26111701; grants from Research on Measures for Intractable Diseases (Ataxic Diseases and Neurodegenerative Diseases) from the Ministry of Health, Labor, and Welfare and the Gunma University Initiative for Advanced Research (GIAR) (to H. Hirai), MEXT KAKENHI grant number 26890005 (to Y. Matsuzaki); and the Brain Sciences Project of the Center for Novel Science Initiatives (CNSI), National Institutes of Natural Sciences (NINS; grant numbers BS251006 and BS261011 to Y. Matsuzaki and A. Konno).

Compliance with Ethical Standards All procedures for the care and treatment of animals were performed in accordance with the Japanese Act on Welfare and Management of Animals, the Guidelines for the Proper Conduct of Animal Experiments by the Science Council of Japan, and the Guide for the Care and Use of Laboratory Animals of the National Research Council of the United States. The experimental protocol was approved by the Institutional Committee of Gunma University (No. 14-039).

Conflict of Interest The authors have no potential conflicts of interest to disclose.

References

1. Kishi N, Sato K, Sasaki E, Okano H (2014) Common marmoset as a new model animal for neuroscience research and genome editing

technology. Develop Growth Differ 56(1):53–62. doi:10.1111/dgd.12109
2. Cox TM, Cachon-Gonzalez MB (2012) The cellular pathology of lysosomal diseases. J Pathol 226(2):241–254. doi:10.1002/path.3021
3. Noh H, Lee JI (2014) Current and potential therapeutic strategies for mucopolysaccharidoses. J Clin Pharm Ther 39(3):215–224. doi:10.1111/jcpt.12136
4. Kesidou E, Lagoudaki R, Touloumi O, Poulatsidou KN, Simeonidou C (2013) Autophagy and neurodegenerative disorders. Neural RegenRes 8(24):2275–2283. doi:10.3969/j.issn.1673-5374.2013.24.007
5. Roussel BD, Kruppa AJ, Miranda E, Crowther DC, Lomas DA, Marciniak SJ (2013) Endoplasmic reticulum dysfunction in neurological disease. Lancet Neurol 12(1):105–118. doi:10.1016/S1474-4422(12)70238-7
6. Ward SM, Himmelstein DS, Lancia JK, Binder LI (2012) Tau oligomers and tau toxicity in neurodegenerative disease. Biochem Soc Trans 40(4):667–671. doi:10.1042/BST20120134
7. Nobrega C, Nascimento-Ferreira I, Onofre I, Albuquerque D, Hirai H, Deglon N, de Almeida LP (2013) Silencing mutant ataxin-3 rescues motor deficits and neuropathology in Machado-Joseph disease transgenic mice. PLoS One 8(1):e52396. doi:10.1371/journal.pone.0052396
8. Iwata N, Sekiguchi M, Hattori Y, Takahashi A, Asai M, Ji B, Higuchi M, Staufenbiel M et al (2013) Global brain delivery of neprilysin gene by intravascular administration of AAV vector in mice. Sci Rep 3:1472. doi:10.1038/srep01472
9. Torashima T, Koyama C, Iizuka A, Mitsumura K, Takayama K, Yanagi S, Oue M, Yamaguchi H et al (2008) Lentivector-mediated rescue from cerebellar ataxia in a mouse model of spinocerebellar ataxia. EMBO Rep 9(4):393–399. doi:10.1038/embor.2008.31
10. Flotte TR (2000) Size does matter: overcoming the adeno-associated virus packaging limit. Respir Res 1(1):16–18. doi:10.1186/rr6
11. Murlidharan G, Samulski RJ, Asokan A (2014) Biology of adeno-associated viral vectors in the central nervous system. Front Mol Neurosci 7:76. doi:10.3389/fnmol.2014.00076
12. Masamizu Y, Okada T, Kawasaki K, Ishibashi H, Yuasa S, Takeda S, Hasegawa I, Nakahara K (2011) Local and retrograde gene transfer into primate neuronal pathways via adeno-associated virus serotype 8 and 9. Neuroscience 193:249–258. doi:10.1016/j.neuroscience.2011.06.080
13. Bevan AK, Duque S, Foust KD, Morales PR, Braun L, Schmelzer L, Chan CM, McCrate M et al (2011) Systemic gene delivery in large species for targeting spinal cord, brain, and peripheral tissues for pediatric disorders. Mol Ther 19(11):1971–1980. doi:10.1038/mt.2011.157
14. Gray SJ, Matagne V, Bachaboina L, Yadav S, Ojeda SR, Samulski RJ (2011) Preclinical differences of intravascular AAV9 delivery to neurons and glia: a comparative study of adult mice and nonhuman primates. Mol Ther 19(6):1058–1069. doi:10.1038/mt.2011.72
15. Gray SJ, Nagabhushan Kalburgi S, McCown TJ, Jude Samulski R (2013) Global CNS gene delivery and evasion of anti-AAV-neutralizing antibodies by intrathecal AAV administration in non-human primates. Gene Ther 20(4):450–459. doi:10.1038/gt.2012.101
16. Hinderer C, Bell P, Vite CH, Louboutin JP, Grant R, Bote E, Yu H, Pukenas B et al (2014) Widespread gene transfer in the central nervous system of cynomolgus macaques following delivery of AAV9 into the cisterna magna. Mol Ther Methods Clin Dev 1:14051. doi:10.1038/mtm.2014.51
17. Meyer K, Ferraiuolo L, Schmelzer L, Braun L, McGovern V, Likhite S, Michels O, Govoni A et al (2015) Improving single injection CSF delivery of AAV9-mediated gene therapy for SMA: a dose–response study in mice and nonhuman primates. Mol Ther 23(3):477–487. doi:10.1038/mt.2014.210
18. Samaranch L, Salegio EA, San Sebastian W, Kells AP, Bringas JR, Forsayeth J, Bankiewicz KS (2013) Strong cortical and spinal cord transduction after AAV7 and AAV9 delivery into the cerebrospinal fluid of nonhuman primates. Hum Gene Ther 24(5):526–532. doi:10.1089/hum.2013.005
19. Samaranch L, Salegio EA, San Sebastian W, Kells AP, Foust KD, Bringas JR, Lamarre C, Forsayeth J et al (2012) Adeno-associated virus serotype 9 transduction in the central nervous system of non-human primates. Hum Gene Ther 23(4):382–389. doi:10.1089/hum.2011.200
20. Yoon SY, Bagel JH, O'Donnell PA, Vite CH, Wolfe JH (2015) Clinical improvement of alpha-mannosidosis cat following a single cisterna magna infusion of AAV1. Mol Ther. doi:10.1038/mt.2015.168
21. Matsuzaki Y, Oue M, Hirai H (2014) Generation of a neurodegenerative disease mouse model using lentiviral vectors carrying an enhanced synapsin I promoter. J Neurosci Methods 223:133–143. doi:10.1016/j.jneumeth.2013.12.004
22. Loeb JE, Cordier WS, Harris ME, Weitzman MD, Hope TJ (1999) Enhanced expression of transgenes from adeno-associated virus vectors with the woodchuck hepatitis virus posttranscriptional regulatory element: implications for gene therapy. Hum Gene Ther 10(14):2295–2305. doi:10.1089/10430349950016942
23. Koeppen AH (2005) The pathogenesis of spinocerebellar ataxia. Cerebellum 4(1):62–73. doi:10.1080/14734220510007950
24. Seki T, Adachi N, Abe-Seki N, Shimahara T, Takahashi H, Yamamoto K, Saito N, Sakai N (2011) Elucidation of the molecular mechanism and exploration of novel therapeutics for spinocerebellar ataxia caused by mutant protein kinase C gamma. J Pharmacol Sci 116(3):239–247
25. Zhang Y, Kaczmarek LK (2015) Kv3.3 potassium channels and spinocerebellar ataxia. J Physiol. doi:10.1113/JP271343
26. Takayama K, Torashima T, Horiuchi H, Hirai H (2008) Purkinje-cell-preferential transduction by lentiviral vectors with the murine stem cell virus promoter. Neurosci Lett 443(1):7–11. doi:10.1016/j.neulet.2008.07.058
27. Gallay MN, Jeanmonod D, Liu J, Morel A (2008) Human pallidothalamic and cerebellothalamic tracts: anatomical basis for functional stereotactic neurosurgery. Brain Struct Funct 212(6):443–463. doi:10.1007/s00429-007-0170-0
28. Vaudano E, Legg CR (1992) Cerebellar connections of the ventral lateral geniculate nucleus in the rat. Anat Embryol 186(6):583–588
29. Glickstein M (2000) How are visual areas of the brain connected to motor areas for the sensory guidance of movement? Trends Neurosci 23(12):613–617
30. Huda F, Konno A, Matsuzaki Y, Goenawan H, Miyake K, Shimada T, Hirai H (2014) Distinct transduction profiles in the CNS via three injection routes of AAV9 and the application to generation of a neurodegenerative mouse model. Mol Ther Methods Clin Dev. Article number: 14032. doi:10.1038/mtm.2014.32
31. Kirik D, Bjorklund A (2003) Modeling CNS neurodegeneration by overexpression of disease-causing proteins using viral vectors. Trends Neurosci 26(7):386–392. doi:10.1016/S0166-2236(03)00164-4
32. Wolf DA, Banerjee S, Hackett PB, Whitley CB, McIvor RS, Low WC (2015) Gene therapy for neurologic manifestations of mucopolysaccharidoses. Expert Opin Drug Deliv 12(2):283–296. doi:10.1517/17425247.2015.966682
33. Heldermon CD, Ohlemiller KK, Herzog ED, Vogler C, Qin E, Wozniak DF, Tan Y, Orrock JL et al (2010) Therapeutic efficacy of bone marrow transplant, intracranial AAV-mediated gene therapy, or both in the mouse model of MPS IIIB. Mol Ther 18(5):873–880. doi:10.1038/mt.2010.17

34. Gholizadeh S, Tharmalingam S, Macaldaz ME, Hampson DR (2013) Transduction of the central nervous system after intracerebroventricular injection of adeno-associated viral vectors in neonatal and juvenile mice. Human Gene Ther Methods 24(4): 205–213. doi:10.1089/hgtb.2013.076
35. McLean JR, Smith GA, Rocha EM, Hayes MA, Beagan JA, Hallett PJ, Isacson O (2014) Widespread neuron-specific transgene expression in brain and spinal cord following synapsin promoter-driven AAV9 neonatal intracerebroventricular injection. Neurosci Lett 576:73–78. doi:10.1016/j.neulet.2014.05.044
36. Miyake N, Miyake K, Yamamoto M, Hirai Y, Shimada T (2011) Global gene transfer into the CNS across the BBB after neonatal systemic delivery of single-stranded AAV vectors. Brain Res 1389: 19–26. doi:10.1016/j.brainres.2011.03.014
37. Abbott NJ (2004) Evidence for bulk flow of brain interstitial fluid: significance for physiology and pathology. Neurochem Int 45(4): 545–552. doi:10.1016/j.neuint.2003.11.006
38. Koh L, Zakharov A, Johnston M (2005) Integration of the subarachnoid space and lymphatics: is it time to embrace a new concept of cerebrospinal fluid absorption? Cerebrospinal Fluid Res 2:6. doi: 10.1186/1743-8454-2-6
39. Praetorius J (2007) Water and solute secretion by the choroid plexus. Pflugers Arch - Eur J Physiol 454(1):1–18. doi:10.1007/s00424-006-0170-6
40. Iliff JJ, Wang M, Liao Y, Plogg BA, Peng W, Gundersen GA, Benveniste H, Vates GE et al (2012) A paravascular pathway facilitates CSF flow through the brain parenchyma and the clearance of interstitial solutes, including amyloid beta. Sci Transl Med 4(147):147ra111. doi:10.1126/scitranslmed.3003748
41. Oberheim NA, Takano T, Han X, He W, Lin JH, Wang F, Xu Q, Wyatt JD et al (2009) Uniquely hominid features of adult human astrocytes. J Neurosci 29(10):3276–3287. doi:10.1523/JNEUROSCI.4707-08.2009
42. Federici T, Taub JS, Baum GR, Gray SJ, Grieger JC, Matthews KA, Handy CR, Passini MA et al (2012) Robust spinal motor neuron transduction following intrathecal delivery of AAV9 in pigs. Gene Ther 19(8):852–859. doi:10.1038/gt.2011.130
43. Torashima T, Okoyama S, Nishizaki T, Hirai H (2006) In vivo transduction of murine cerebellar Purkinje cells by HIV-derived lentiviral vectors. Brain Res 1082(1):11–22. doi:10.1016/j.brainres.2006.01.104
44. Konno A, Shuvaev AN, Miyake N, Miyake K, Iizuka A, Matsuura S, Huda F, Nakamura K et al (2014) Mutant ataxin-3 with an abnormally expanded polyglutamine chain disrupts dendritic development and metabotropic glutamate receptor signaling in mouse cerebellar Purkinje cells. Cerebellum 13(1):29–41. doi:10.1007/s12311-013-0516-5
45. Miyake K, Miyake N, Yamazaki Y, Shimada T, Hirai Y (2012) Serotype-independent method of recombinant adeno-associated virus (AAV) vector production and purification. J Nippon Med School = Nippon Ika Daigaku zasshi 79(6):394–402